Supporting Information for

Global evaluation of ELMv1-CNP and the role of the phosphorus cycle in the historical terrestrial carbon balance

Xiaojuan Yang[1*], Peter Thornton[1], Daniel Ricciuto[1], Yilong Wang[2,3], Forrest Hoffman[4]

[1]Environmental Sciences Division, Oak Ridge National Lab, Oak Ridge, TN 37831

[2]Key Laboratory of Land Surface Pattern and Simulation, Institute of Geographic Sciences and Natural Resources Research, Chinese Academy of Sciences, Beijing, China

[3]Laboratoire des Sciences du Climat et de l'Environnement, CEA-CNRS-UVSQ- Université Paris Saclay, 91191, Gif-sur-Yvette CEDEX, France

[4]Computational Sciences & Engineering Division, Oak Ridge National Lab, Oak Ridge, TN 37831

Contents of this file

Introduction

This supporting information provides supplementary text, figures and tables for the main article.

Text S1: Additional description of the representation of Non-structural (NSC) pool in ELMv1-CNP

In the current model configuration, there are no direct feedbacks of the non-structural carbon pool on plant activities. When soil nutrient supply is high, allocation to new NSC decreases and allocation to biomass construction increases, and the size of the NSC pool declines; however, existing NSC turns over to the atmosphere and is not utilized by plants.

The respiration from the NSC pool R_{NSC} is calculated using the following equation:

$$R_{NSC} = br_{cpool} * C_{NSC} * Q_{10}^{(Tair-298.15)/10}$$

Where br_{cpool} is the respiration base rate at 25°C, which is set to 10^{-9} gC m^{-2} s^{-1}. This is equivalent to roughly a 3-year turnover time for the NSC pool C_{NSC}, which is broadly consistent with observations that indicate a range of values across plant components and NSC forms with a weighted mean of 2-3 years (Richardson et al., 2015). The Q_{10} parameter, which has a value of 1.5 in these simulations, controls the strength of the temperature response. T_{air} is the 2-meter air temperature (K).

Nutrients are allocated from the non-structural pools using the following equation:

$$N_{alloc} = \frac{N_{demand}}{max\left(\frac{N_{NS,max}}{N_{NS}}, 1\right)}$$

Where N_{demand} is the amount of nutrient (nitrogen or phosphorus) required to allocate all NPP during a model timestep to plant structural pools given the stoichiometry. N_{NS} is the size of the non-structural nutrient pool, and $N_{NS,max}$ is the size of the pool above which there is no nutrient limitation.

$$N_{NS,max} = Nstor * NPP_{N,anual}$$

$NPP_{N,annual}$ is the previous year's total of annual net primary productivity for the nutrient of interest. The parameter *Nstor* is set to 3 for these simulations. Therefore, nutrient limitation only affects allocation when there are less than 3 years of non-structural nutrient storage. This is consistent with the average age of NSC found by (Richardson et al., 2015), though that analysis found a 2-pool NSC model may have more predictive skill, which we will consider implementing in future work.

These computations of N_{alloc} are done for both nitrogen and phosphorus. The actual allocation of carbon, nitrogen and phosphorus is set by whichever nutrient is more limiting at that timestep given the lower of the ratios N_{alloc}:N_{demand}.

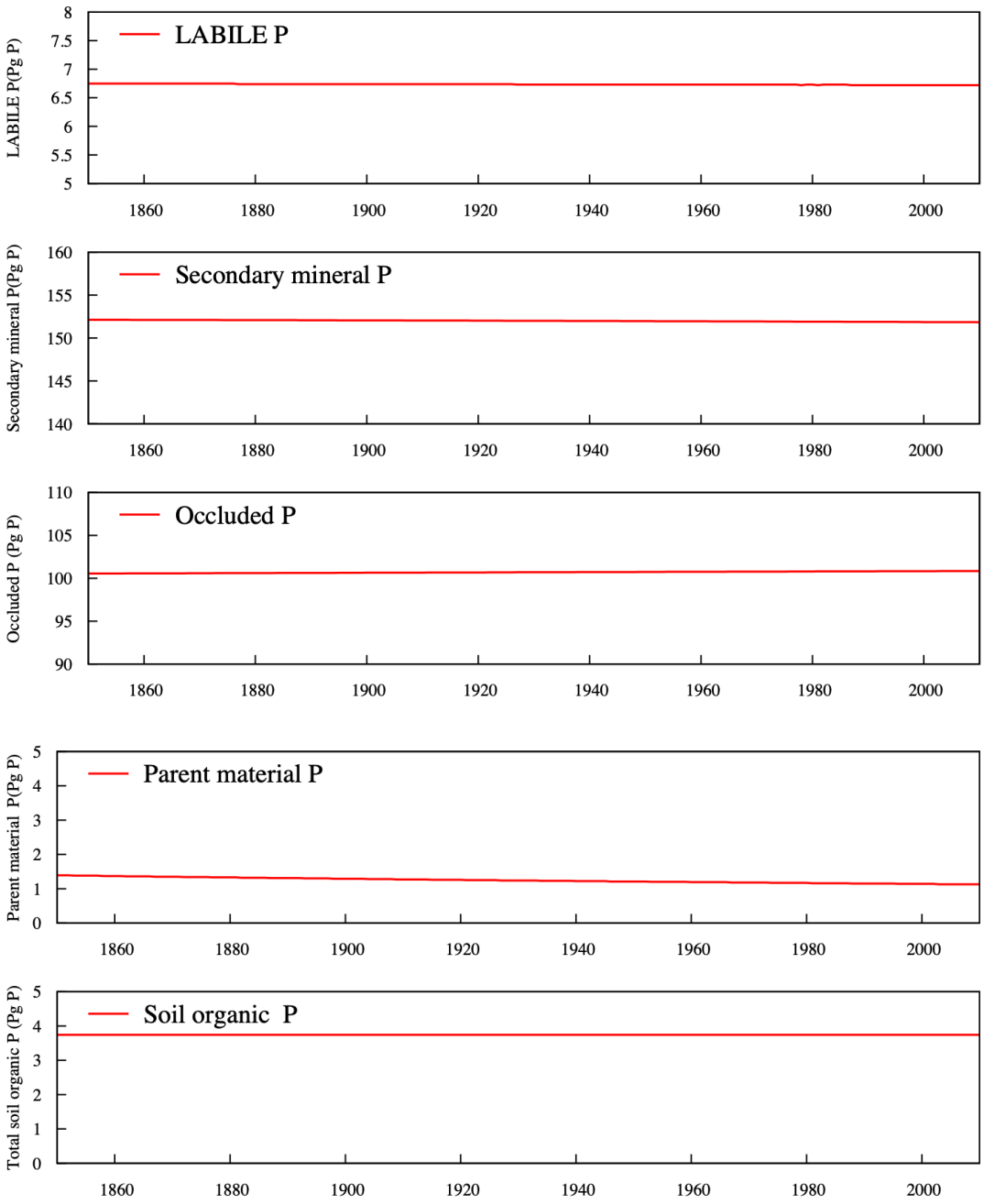

Figure S1: Time series of globally-integrated P pools for the control run, which is the continuation of the normal spinup.

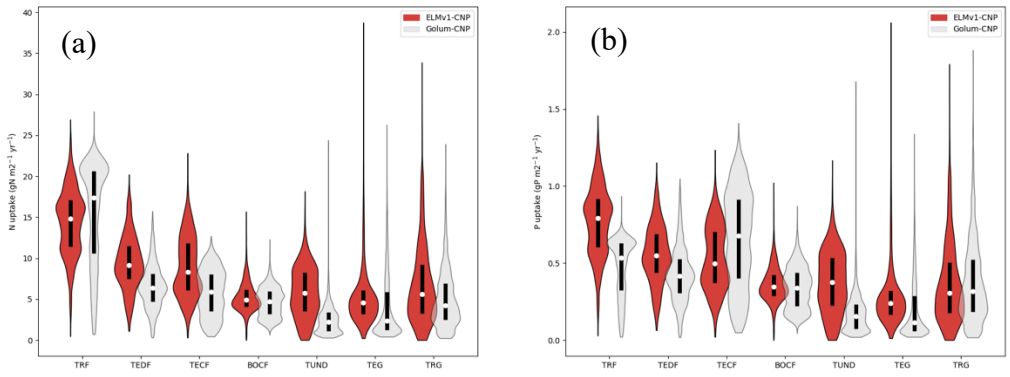

Figure S2: Violin plots of (a) nitrogen uptake (g N m^{-2} yr^{-1}) and (b) phosphorus uptake (g P m^{-2} yr^{-1}) from ELMv1-CNP and GOLUM-CNP for seven biomes: tropical rainforest (TRF), temperate deciduous forest (TEDF), temperate coniferous forest (TECF), boreal coniferous forest (BOCF), temperate grassland (TEG) and tropical grassland (TRG). Plots show the medians of all grid cells in each biome (open circles) and the probability density distribution (balloons).

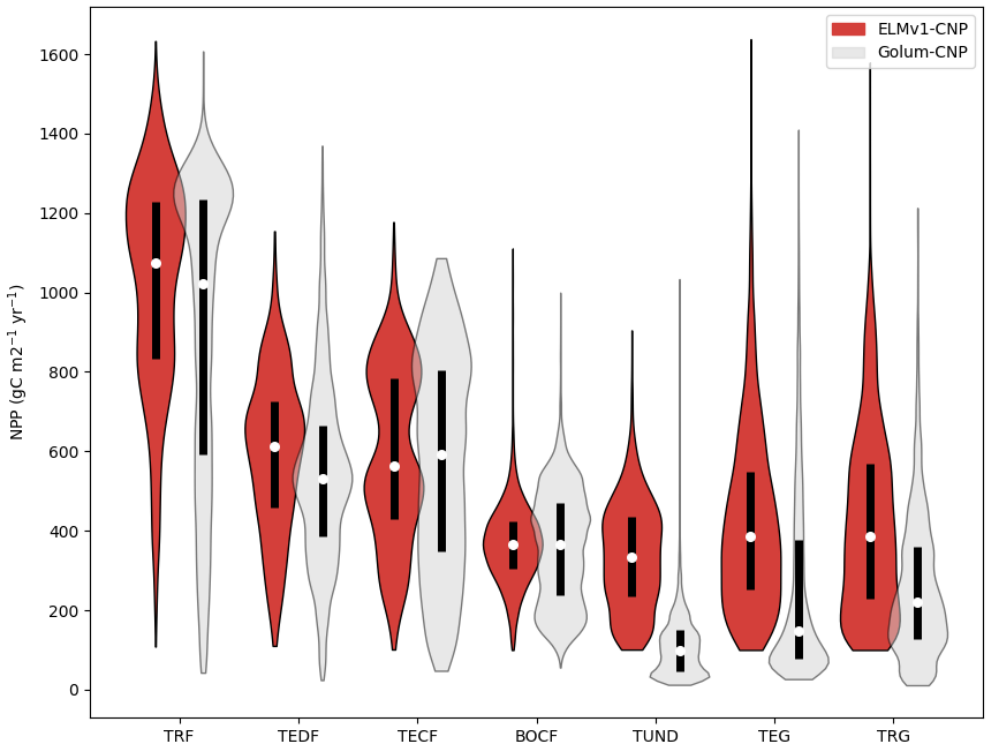

Figure S3: Violin plots of NPP (g C m^{-2} yr^{-1}) from ELMv1-CNP and GOLUM-CNP for seven biomes: tropical rainforest (TRF), temperate deciduous forest (TEDF), temperate coniferous forest (TECF), boreal coniferous forest (BOCF), temperate grassland (TEG) and tropical grassland (TRG). Plots show the medians of all grid cells in each biome (open circles) and the probability density distribution (balloons).

(a)

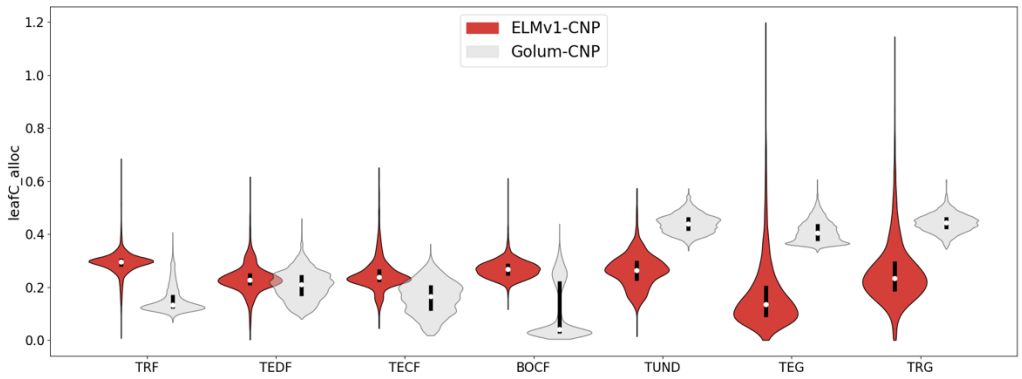

Figure S4:: Violin plots of NPP allocation fractions to leaf from ELMv1-CNP and GOLUM-CNP for seven biomes: tropical rainforest (TRF), temperate deciduous forest (TEDF), temperate coniferous forest (TECF), boreal coniferous forest (BOCF), temperate grassland (TEG) and tropical grassland (TRG). Plots show the medians of all grid cells in each biome (open circles) and the probability density distribution (balloons).

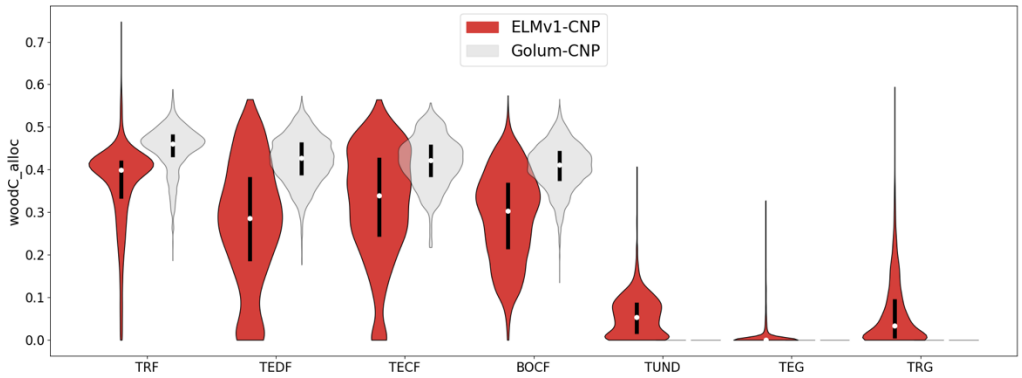

Figure S5:: Violin plots of NPP allocation fractions to wood from ELMv1-CNP and GOLUM-CNP for seven biomes: tropical rainforest (TRF), temperate deciduous forest (TEDF), temperate coniferous forest (TECF), boreal coniferous forest (BOCF), temperate grassland (TEG) and tropical grassland (TRG). Plots show the medians of all grid cells in each biome (open circles) and the probability density distribution (balloons).

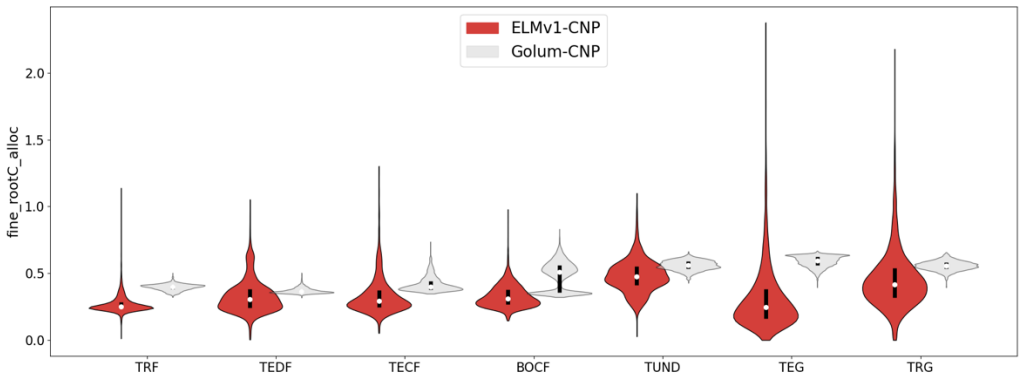

Figure S6: Violin plots of NPP allocation fractions to fine root from ELMv1-CNP and GOLUM-CNP for seven biomes: tropical rainforest (TRF), temperate deciduous forest (TEDF), temperate coniferous forest (TECF), boreal coniferous forest (BOCF), temperate grassland (TEG) and tropical grassland (TRG). Plots show the medians of all grid cells in each biome (open circles) and the probability density distribution (balloons).

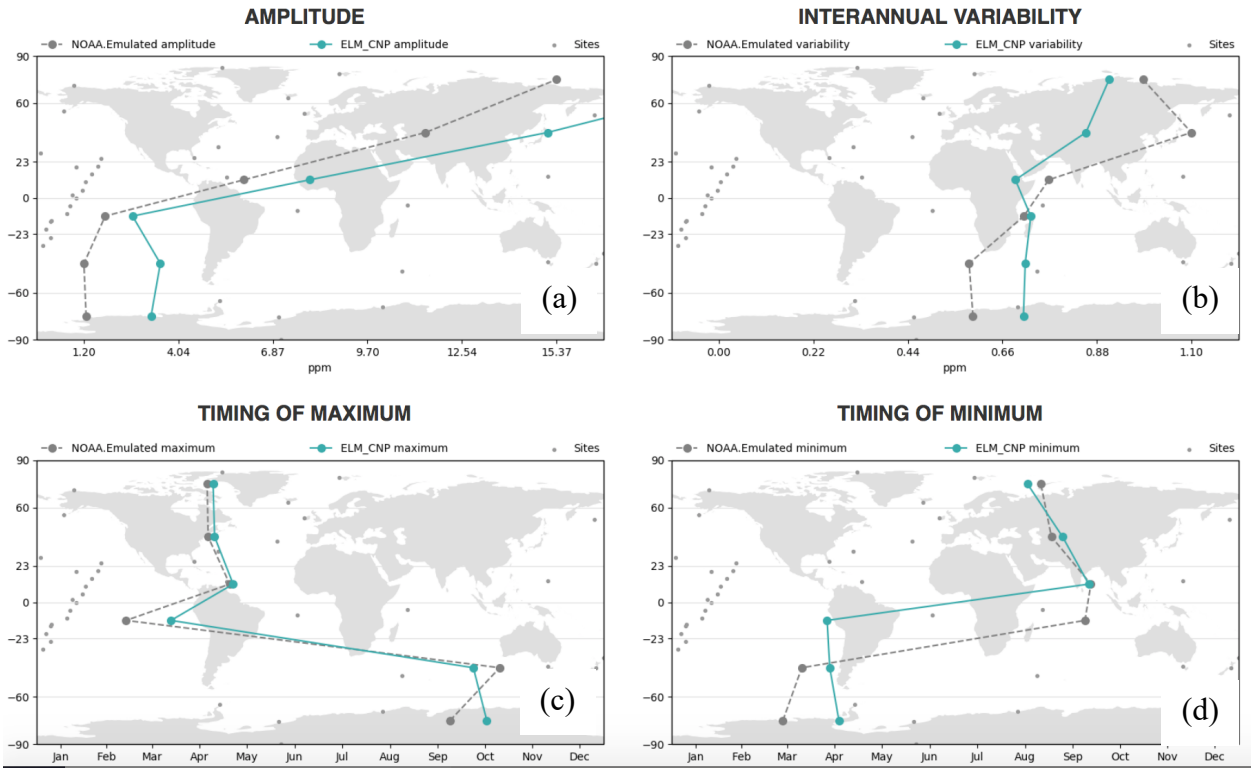

Figure S7: The comparison of atmospheric CO_2 concentrations inferred from ELM v1-CNP land-carbon fluxes (green lines) with in situ flask measurements from NOAA's global Cooperative Air Sampling Network (gray lines) in ILAMB: (a) the mean seasonal amplitude over flask sites [ppm], (b) the range of interannual variability [ppm], (c) the average month-of-year when the peak CO2 concentration occurs, and (d) the average month-of-year when the lowest CO2 concentration occurs. Observations and measurements are binned within 30◦ latitude increments; small gray dots indicate individual flask sampling locations.

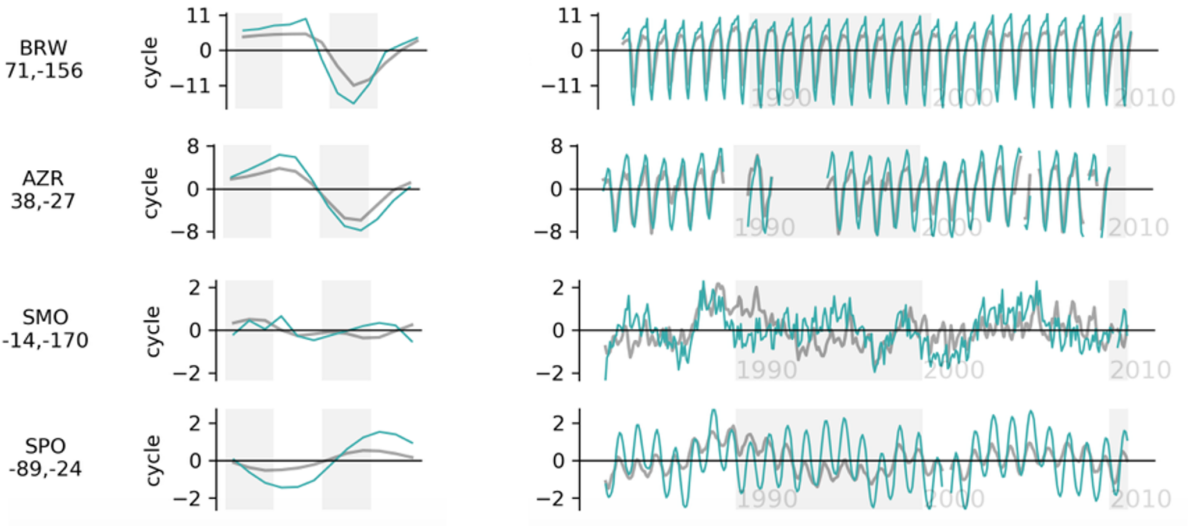

Figure S8: The comparison of atmospheric CO_2 concentrations [ppm] inferred from ELM v1-CNP land-carbon fluxes (green lines) with in situ flask measurements from NOAA's global Cooperative Air Sampling Network (gray lines) in ILAMB: Mean seasonal cycles (left) and full time series (right) for four flask sites: (d) Barrow (71° N, 156 ° W), (e) Azores (38° N, 27 ° W), (f) Samoa (14 ° S, 170 ° W), and (g) South Pole (89 ° S, 24 ° W). Grey shading in the seasonal cycle plots (left) is meant to show the magnitude of seasonality. Grey shading in the time series plots (right) is to show the decades (e.g. 1990 -2000).

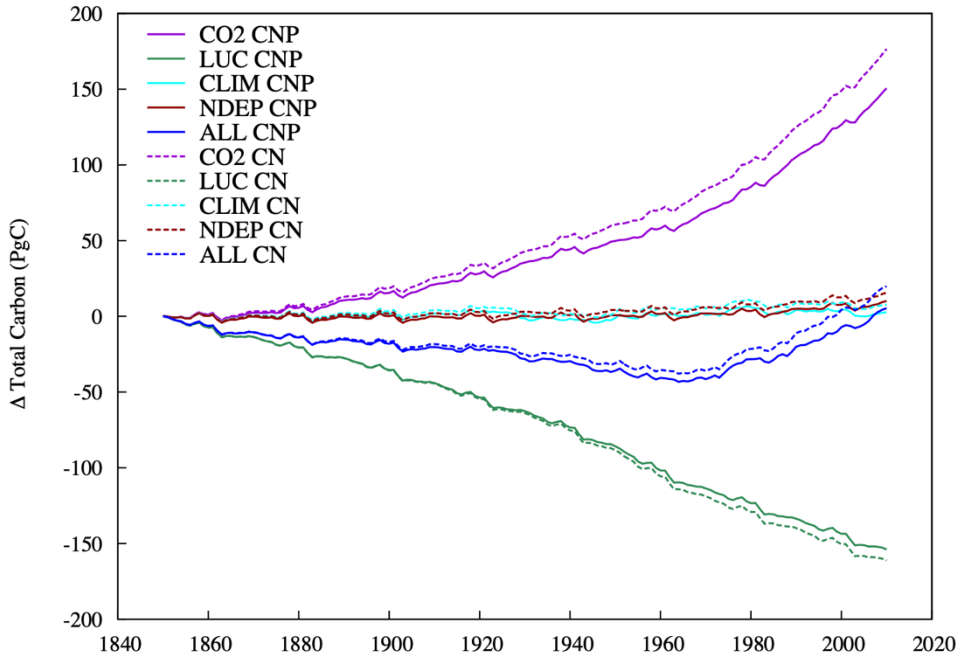

Figure S9: Simulated change in land carbon storage in response to changes in CO2, land use and land cover change, N deposition, climate during 1850-2010. Unit: Pg C. CN is for ELMv1-CN and CNP is for ELMv1-CNP

Table S1: PFT dependent parameters*

PFT	Leaf C:N	Leaf C:P	Fine root C:N	Fine root C:P	Live wood C:N	live wood C:P	Dead wood C:N	Dead wood C:P
Needleleaf evergreen tree - temperate	35	525	42	1000	50	3000	500	3000
Needleleaf evergreen tree - boreal	40	400	42	1000	50	3000	500	3000
Needleleaf deciduous tree - boreal	25	250	42	1000	50	3000	500	3000
Broadleaf evergreen tree - tropical	30	600	42	1000	50	3000	500	3000
Broadleaf evergreen tree - temperate	30	450	42	1000	50	3000	500	3000
Broadleaf deciduous tree - tropical	25	500	42	1000	50	3000	500	3000
Broadleaf deciduous tree - temperate	25	375	42	1000	50	3000	500	3000
Broadleaf deciduous tree - boreal	25	250	42	1000	50	3000	500	3000
Broadleaf evergreen shrub - temperate	30	450	42	1000	50	3000	500	3000
Broadleaf deciduous shrub - temperate	25	375	42	1000	50	3000	500	3000
Broadleaf deciduous shrub - boreal	25	250	42	1000	50	3000	500	3000
C3 arctic	25	250	42	1000				
C3 grass	25	375	42	1000				
C4 grass	25	375	42	1000				

*The sources of the parameters are provided in detail in the supporting information of Yang et al. (2016)

Table S2: Soil order dependent parameters*

	S_{max}	K_s	r_adsorp	r_desorp	r_weathering	R_occlusion
Andisol	1000	0.6	0.005	0.00022	0.005	1e-6
Gelisol	500	0.6	0.005	0.00022	0.001	1e-6
Histosol	500	0.6	0.005	0.00022	0.001	1e-6
Entisol	432	0.49	0.005	0.00022	0.001	1e-6
Inceptisol	500	0.6	0.005	0.00022	0.001	1e-6
Aridsol	700	0.3	0.005	0.00022	0.001	1e-6
Vertisol	700	0.3	0.005	0.00022	0.001	1e-6
Mollisol	700	0.3	0.005	0.00022	0.001	1e-6
Alfisol	700	0.06	0.005	0.00022	0.001	1e-6
Spodosol	925	0.03	0.005	0.00022	0.001	1e-6
Ultisol	1000	0.03	0.004	0.00022	0.0001	1e-6
Oxisol	1000	0.03	0.004	0.00022	0.0001	1e-6

*The sources of the parameters are provided in detail in the supporting information of Yang et al. (2016)

Table S3: List of Input Data

	Input data	Reference
Meteorological forcing	The Global Soil Wetness Project forcing dataset (GSWP3)	http://hydro.iis.u-tokyo.ac.jp/GSWP3/
Land use change	Land-Use harmonization data set (LUH2)	Hurtt et al., 2020
N deposition		Hegglin et al., 2016
CO_2		Meinshausen et al., 2017
P deposition		Mahowald et al. (2008)
Soil P maps	Global maps of different P pools	Yang et al. (2013)

Table S4: Observational Dataset Used for Carbon Cycle Evaluation in ILAMB

Variable	Datasets	References
Biomass	GEOCARBON	Saatchi et al.,2011
	NBCD2000	Kellndorfer et al., 2013
	USForest	Blackard et al., 2008
Burned area	GFED4S	Giglio et al., 2010
Carbon dioxide	NOAA.Emulated	Dlugokencky et al., 2020
Gross primary productivity	Fluxnet	Lasslop et al., 2010
	GBAF	Jung et al., 2011
Leaf area index	AVHRR	Myneni et al., 1997
	MODIS	De Kauwe et al., 2011
Global Net Ecosystem Carbon Balance	GCP	Le Quere et al., 2016
	Hoffman	Hoffman et al., 2014
Net ecosystem exchange	Fluxnet	Lasslop et al., 2010
	GBAF	Jung et al., 2010
Ecosystem respiration	Fluxnet	Lasslop et al., 2010
	GBAF	Jung et al., 2010
Soil carbon	HWSD	Todd-Brown et al., 2013
	NCSCDV22	Hugelius et al., 2013
	Koven	Koven et al., 2017

Reference:

Blackard, J., Finco, M., Helmer, E., Holden, G., Hoppus, M., Jacobs, D., . . . Riemann, R. (2008). Mapping US forest biomass using nationwide forest inventory data and moderate resolution information. *Remote Sensing of Environment, 112*(4), 1658-1677.

De Kauwe, M. G., Disney, M., Quaife, T., Lewis, P., & Williams, M. (2011). An assessment of the MODIS collection 5 leaf area index product for a region of mixed coniferous forest. *Remote Sensing of Environment, 115*(2), 767-780.

Dlugokencky, E.J., J.W. Mund, A.M. Crotwell, M.J. Crotwell, and K.W. Thoning (2020), Atmospheric Carbon Dioxide Dry Air Mole Fractions from the NOAA GML Carbon Cycle Cooperative Global Air Sampling Network, 1968-2019, Version: 2020-07, https://doi.org/10.15138/wkgj-f215

Giglio, L., Randerson, J., Van der Werf, G., Kasibhatla, P., Collatz, G., Morton, D., & DeFries, R. (2010). Assessing variability and long-term trends in burned area by merging multiple satellite fire products. *Biogeosciences, 7*(3), 1171-1186.

Hegglin, M., Kinnison, D., & Lamarque, J.-F. (2016). CCMI nitrogen surface fluxes in support of CMIP6-version 2.0. Earth System Grid Federation. https://doi.org/10.22033/ESGF/input4MIPs.1125

Hoffman, F. M., Randerson, J. T., Arora, V. K., Bao, Q., Cadule, P., Ji, D., . . . Lindsay, K. (2014). Causes and implications of persistent atmospheric carbon dioxide biases in Earth System Models. *Journal of Geophysical Research: Biogeosciences, 119*(2), 141-162.

Hugelius, G., Bockheim, J. G., Camill, P., Elberling, B., Grosse, G., Harden, J. W., . . . Kuhry, P. (2013). A new data set for estimating organic carbon storage to 3 m depth in soils of the northern circumpolar permafrost region. *Earth System Science Data (Online), 5*(2).

Hurtt, G. C., Chini, L., Sahajpal, R., Frolking, S., Bodirsky, B. L., Calvin, K., . . . Goldewijk, K. K. (2020). Harmonization of global land-use change and management for the period 850–2100 (LUH2) for CMIP6. *Geoscientific Model Development Discussions*, 1-65.

Jung, C.-G., Shin, H.-J., Park, M.-J., Joh, H.-K., & Kim, S.-J. (2011). Evaluation of MODIS Gross Primary Production (GPP) by Comparing with GPP from CO 2 Flux Data Measured in a Mixed Forest Area. *Journal of the Korean Society of Agricultural Engineers, 53*(2), 1-8.

Kellndorfer, J., Walker, W., Kirsch, K., Fiske, G., Bishop, J., LaPoint, L., . . . Westfall, J. (2013). NACP aboveground biomass and carbon baseline data, V. 2 (NBCD 2000), USA, 2000. *ORNL DAAC*.

Koven, C. D., Hugelius, G., Lawrence, D. M., & Wieder, W. R. (2017). Higher climatological temperature sensitivity of soil carbon in cold than warm climates. *Nature Climate Change, 7*(11), 817-822.

Lasslop, G., Reichstein, M., Papale, D., Richardson, A. D., Arneth, A., Barr, A., . . . Wohlfahrt, G. (2010). Separation of net ecosystem exchange into assimilation and respiration using a light response curve approach: critical issues and global evaluation. *Global change biology, 16*(1), 187-208.

Mahowald, N., Jickells, T. D., Baker, A. R., Artaxo, P., Benitez-Nelson, C. R., Bergametti, G., . . . Herut, B. (2008). Global distribution of atmospheric phosphorus sources, concentrations and deposition rates, and anthropogenic impacts. *Global Biogeochemical Cycles, 22*(4).

Meinshausen, M., Vogel, E., Nauels, A., Lorbacher, K., Meinshausen, N., Etheridge, D. M., Fraser, P. J., Montzka, S. A., Rayner, P. J., Trudinger, C. M., Krummel, P. B., Beyerle,

U., Canadell, J. G., Daniel, J. S., Enting, I. G., Law, R. M., Lunder, C. R., O'Doherty, S., Prinn, R. G., Reimann, S., Rubino, M., Velders, G. J. M., Vollmer, M. K., Wang, R. H. J., and Weiss, R. (2017). Historical greenhouse gas concentrations for climate modelling (CMIP6), Geosci. Model Dev., 10, 2057-2116.

Myneni, R. B., Ramakrishna, R., Nemani, R., & Running, S. W. (1997). Estimation of global leaf area index and absorbed PAR using radiative transfer models. *IEEE Transactions on Geoscience and Remote Sensing, 35*(6), 1380-1393.

Yang, X., Post, W. M., Thornton, P. E., & Jain, A. (2013). The distribution of soil phosphorus for global biogeochemical modeling. *Biogeosciences, 10*(4), 2525-2537. doi:10.5194/bg-10-2525-2013.

Richardson, A. D., Carbone, M. S., Huggett, B. A., Furze, M. E., Czimczik, C. I., Walker, J. C., . . . Murakami, P. (2015). Distribution and mixing of old and new nonstructural carbon in two temperate trees. *New Phytologist, 206*(2), 590-597.

Yang, X., Thornton, P. E., Ricciuto, D. M., & Hoffman, F. M. (2016). Phosphorus feedbacks constraining tropical ecosystem responses to changes in atmospheric CO2 and climate. *Geophysical Research Letters, 43*(13), 7205-7214.